Fundamental Reaction Pathways and Free-Energy Barriers for Ester Hydrolysis of Intracellular Second-Messenger 3′,5′-Cyclic Nucleotide

Xi Chen and Chang-Guo Zhan*

College of Chemistry, Central China Normal University, Wuhan 430079, P. R. China, and Department of Pharmaceutical Sciences, College of Pharmacy, University of Kentucky, 907 Rose Street, Lexington, Kentucky 40536

Received: October 19, 2003; In Final Form: February 24, 2004

We have performed a series of first-principles electronic structure calculations to study competing reaction pathways and the corresponding free-energy barriers for the ester hydrolysis of intracellular second-messenger adenosine 3′,5′-cyclic monophosphate (cAMP) and related phosphodiesters including trimethylene phosphate (TMP). Reaction coordinate calculations show three fundamental reaction pathways for the ester hydrolysis, including (A) attack of a hydroxide ion at the P atom of the phosphate anion (an S_N2 process without a pentacoordinated phosphorus intermediate), (B) direct attack of a water molecule at the P atom of the anion (a three-step process), and (C) direct attack of a water molecule at the P atom of the neutral ester molecule (a two-step process). The calculated energy results show that for the reactions in the gas phase the free-energy barrier for pathway A is the highest and the barrier for the rate-controlling step of pathway C is the lowest. However, for the reactions in aqueous solution, the free-energy barrier calculated for pathway A becomes the lowest, and the two main hydrolysis pathways are A and B. We also have demonstrated how the pK_a of the ester and the pH of the reaction solution affect the relative contributions of different hydrolysis pathways to the total hydrolysis rate. Reaction pathway A should be dominant for the cAMP hydrolysis in neutral aqueous solution. However, the relative contribution of pathway A to the total hydrolysis rate should decrease with decreasing pH of the solution. For pH $< \sim$3.7, the contribution of pathway B is larger. For pH $> \sim$3.7, the contribution of pathway A is larger. The reliability of our theoretical predictions is supported by the excellent agreement of the calculated free-energy barrier with available experimental data for the hydrolysis of TMP in solution.

Introduction

3′,5′-Cyclic nucleotides, such as adenosine 3′,5′-cyclic monophosphate (cAMP) found by Sutherland and Rall nearly a half-century ago,[1] are intracellular second messengers that are essential to vision, muscle contraction, neurotransmission, exocytosis, cell growth, and differentiation.[2] The 3′,5′-cyclic nucleotides (e.g., cAMP) are synthesized by receptor-linked enzymes (such as adenylyl and guanylyl cyclase) and metabolized to the corresponding 5′-nucleotide metabolites (e.g., AMP). The metabolizing pathways include both nonenzymatic and enzymatic ester hydrolysis. The primary metabolizing enzymes for these intracellular second messengers are phosphodiesterases (PDEs), a superfamily of enzymes.[3,4] Hence, PDEs are clinical targets for such biological disorders as retinal degeneration, congestive heart failure, depression, asthma, erectile dysfunction, and inflammation.[5−7] Certain PDE inhibitors have already been shown to or have been expected to exert beneficial effects in a number of therapeutic areas, including stimulation of myocardial contractility, inhibition of mediator release, inhibition of platelet aggregation, cancer chemotherapy, analgesia, treatment of depression, Parkinson's disease, and learning and memory disorders.[8,9] Understanding the fundamental reaction mechanism for the hydrolysis of 3′,5′-cyclic nucleotides will lead to useful insights concerning how to control the concentration of the intracellular second messengers more effectively and therefore provide a solid basis for the rational design of the more-efficient therapeutics.

Concerning the mechanism for PDE-catalyzed hydrolysis, two recently reported 3D X-ray crystal structures[3,4] of PDEs provide a structural basis. The first one is for the catalytic domain of human phosphodiesterase 4B2B (PDE4, cAMP-specific) described by Xu et al.[3] The other is for the catalytic domain of PDE5,[4] which has an active site similar to that of PDE4. For both PDE4 and PDE5, the active site contains a cluster of two divalent metal ions, denoted by Me1 and Me2. Me1 is likely a Zn^{2+} ion based on the observed geometry of the metal-coordinating ligands, the anomalous X-ray diffraction behavior, the existing biochemical evidence,[10−13] and the known high affinity of PDE4 for zinc.[14] Me2 may be Mg^{2+}, Mn^{2+}, or Zn^{2+}, but either Mg^{2+} or Mn^{2+} is the relevant physiological ion.[3] In the PDE4 active site, an Asp-392 residue coordinates to Me1 through an O_δ atom; His-238 and His-274 residues coordinate to Me1 through the N_ϵ atoms; and four solvent water molecules coordinate to Me2 through the O atoms. In addition, there are two bridging ligands. For PDE4, one bridging ligand is clearly Asp-275, whose two O_δ atoms coordinate to Me1 and Me2. However, it was uncertain whether the other bridging ligand is a water molecule or a hydroxide ion because hydrogen atoms cannot be determined by X-ray diffraction techniques. Xu et al.[3] described the second bridging ligand as a water molecule, although it had been clear that the second bridging ligand in the X-ray crystal structure of Zn^{2+}-substituted phosphotriesterase

* To whom all correspondence should be addressed. E-mail: zhan@uky.edu.

10.1021/jp0371635 CCC: $27.50
Published on Web 03/31/2004

(PTE) should be a hydroxide ion.[15] The identity of this second bridging ligand is theoretically determined by performing first-principles quantum chemical calculations on models of the active site.[16] All of the calculated results obtained indicate that this critical second bridging ligand in the active site of the reported X-ray crystal structure of PDE reported by Xu et al. should also be a hydroxide ion, rather than a water molecule, and is expected to serve as the nucleophile to initialize the catalytic hydrolysis of 3′,5′-cyclic nucleotides.[16] This implies that the primary metabolizing pathway of 3′,5′-cyclic nucleotides in PDE should be associated with the ester hydrolysis catalyzed by a hydroxide ion bridging the two metal ions in the PDE active site. Neglecting the two metal ions and the protein environment, the PDE-catalyzed hydrolysis is simplified as the hydroxide ion-catalyzed hydrolysis. This is expected to be similar to the case of the PTE-catalyzed hydrolysis of phosphotriesters and their structural variants.[17]

There is no question that the two metal ions in the PDE active site and the specific PDE protein environment should significantly affect the hydroxide ion-catalyzed hydrolysis. In any case, because the PDE-catalyzed reaction pathway is related to the nonenzymatic reaction pathway in the way mentioned above, it is interesting to first know the fundamental pathways of both the enzymatic and nonenzymatic reactions for the purpose of understanding the function of the enzyme: How do the two metal ions and the protein environment change the reaction pathway for the 3′,5′-cyclic nucleotide hydrolysis in PDE? How much lower is the free-energy barrier for the PDE-catalyzed hydrolysis than that for the corresponding nonenzymatic hydrolysis? So our first step toward understanding the complicated mechanism for the PDE-catalyzed hydrolysis of intracellular second messengers is to study possible fundamental reaction pathways for the nonenzymatic hydrolysis of the 3′,5′-cyclic nucleotide.

Concerning nonenzymatic hydrolysis of organophosphate in aqueous solution, it has been considered that the hydrolysis of the monoesters proceeds by a dissociative, unimolecular elimination pathway, whereas the hydrolysis of the diesters and triesters follow a bimolecular base-catalyzed hydrolysis mechanism.[18−20] The bimolecular base-catalyzed hydrolysis is initialized by the nucleophilic attack of the hydroxide ion at the phosphorus atom of the ester. However, Florian and Warshel et al.[21,22] recently questioned a long-standing mechanistic postulate for the phosphate monoester hydrolysis mechanism. They reexamined the available experimental data and found that although the experimental results for solution reactions had usually been considered to be evidence of the dissociative pathway a closer thermodynamic analysis of observed linear free-energy relationships showed that the experimental information is consistent with the associative, concerted, and dissociative alternatives.[22] So it is currently not clear which reaction pathway dominates the hydrolysis of the monoesters. Their work clearly illustrates that reliable computational studies of fundamental reaction pathways and the corresponding energetics are necessary even for chemical reactions in solution that have been thoroughly investigated by experiment. Florian and Warshel further reported a systematic theoretical study of the nonenzymatic hydrolysis of monomethyl phosphate via the nucleophilic attack at the phosphorus center and explored the energetics of various reaction intermediates and transition states.[23] This systematic study not only provided insight into the competing reaction pathways for the monoester hydrolysis but also demonstrated a useful computational approach to addressing the mechanistic questions for the hydrolysis in solution. The general philosophy of the computational approach was also extended to simulate the competing reaction pathways for the chemical catalysis of DNA polymerases.[24]

Theoretical studies on the hydrolysis mechanism of phosphotriester paraoxon and the structural variants (new molecules)[17] reveal that in the nucleophilic reaction the hydroxide ion is positioned near the extension line of the departing oxygen atom and the phosphorus center. The calculated results also indicate that the hydroxide ion-catalyzed hydrolysis involves a pentacoordinated phosphorus intermediate for all examined compounds, except paraoxon. For paraoxon, the expected pentacoordinated phosphorus intermediate does not exist, and the hydroxide ion-catalyzed hydrolysis is a single-step process such as an S_N2 process.[17] A series of ab initio electronic structure calculations on the reactions of hydroxide/hydroxyl ion with phosphodiesters and other related phosphate esters in the gas phase and in solution have been reported by Lim et al.[25−30] Their gas-phase calculations[25,26] suggest that a dianionic pentacoordinated phosphorus intermediate either does not exist or is only marginally stable, whereas a singly charged pentacoordinated phosphorus intermediate could exist during the reaction process. Taira et al.[31] also performed ab initio calculations at the HF/3-21+G(*) and HF/6-31+G(d) levels to study the thermodynamic stability of the dianionic pentacoordinated phosphorus intermediates and indicated that the dianionic pentacoordinated phosphorus intermediates could exist under certain reaction conditions. Dejaegere, Karplus, and co-workers[32−34] performed ab initio electronic structure calculations to study the hydroxide ion-catalyzed hydrolysis of a cyclic ethylene phosphate (EP) and an acyclic dimethyl phosphate (DMP) to understand the remarkable hydrolysis rate difference between cyclic and acyclic phosphodiesters. They examined the effects of solvation and ring strain on the free-energy barrier for the first step of the reaction and concluded that the difference in the hydrolysis rate between cyclic and acyclic phosphodiesters is primarily due to solvation rather than ring strain.[32] We note that the free-energy barrier difference between the hydrolysis of cyclic and acyclic phosphodiesters is relatively small compared to the high energetics of the overall hydrolysis process. Dejaegere, Karplus, and co-workers never tried to examine the dissociative pathway of the hydrolysis. Because they examined only the structures of the reactants and first transition states, it is not clear whether the hydroxide ion-catalyzed hydrolysis of these phosphodiesters is a one-step or a two-step process. A two-step process should involve a pentacoordinated phosphorus intermediate. Florian, Goodman, and Warshel recently examined the free-energy surface for the DMP hydrolysis in solution at the MP2/6-31+G(d,p)//6-31G(d) level. Their geometry optimization in solution did not lead to a stable dianionic pentacoordinate intermediate. However, whether a pentacoordinated phosphorus intermediate exists or not should be dependent on the specific ester in light of our previously reported results for phosphotriester paraoxon and the structural variants.[17] So both the one- and two-step processes are possible for cAMP and related phosphodiesters.

In addition, no alternative reaction pathway was examined for the hydrolysis of any phosphodiester in previously reported reaction coordinate calculations. We note that although Dejaegere and Karplus et al.'s results of the calculations on the hydroxide ion-catalyzed hydrolysis of EP and DMP can satisfactorily explain the significant hydrolysis rate difference between these two phophodiesters their calculated activation free energy in solution (∼38 kcal/mol for DMP) is significantly higher than the corresponding experimental estimate (32 kcal/

SCHEME 1: Hydrolysis of cAMP and Its Protonated Form

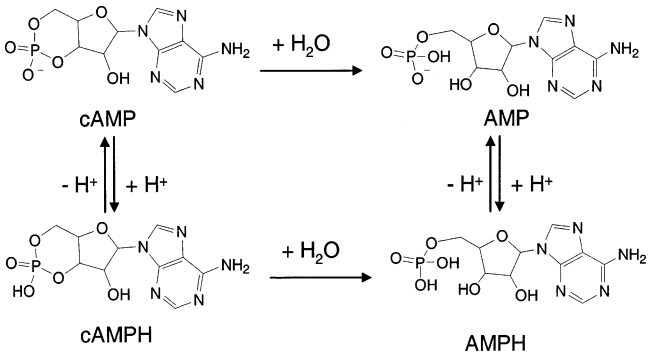

mol for DMP).[32] The deviation of ∼6 kcal/mol tells us that either their electronic structure calculations, particularly the solvation calculations, are not sufficiently accurate or there exists another reaction pathway with a lower activation free energy. The answer to this question remains unknown without performing further computational studies with a more reliable solvation model on possible competing reaction pathways.

In principle, the hydrolysis of a phosphodiester (e.g., cAMP) in water (at pH 7) could involve the following possible pathways, assuming that acid-catalyzed hydrolysis pathways can be ignored:

$$\text{cAMP}^-(\text{anion}) + \text{HO}^- \rightarrow \text{product} \quad (1)$$

$$\text{cAMP}^-(\text{anion}) + \text{H}_2\text{O} \rightarrow \text{product} \quad (2)$$

$$\text{cAMPH(neutral)} + \text{HO}^- \rightarrow \text{product} \quad (3)$$

$$\text{cAMPH(neutral)} + \text{H}_2\text{O} \rightarrow \text{product} \quad (4)$$

Here we use cAMPH to represent the protonated form (a neutral species) of cAMP. See Scheme 1 for the molecular structures. We note that reactions 1 and 2 represent two different reaction pathways, although these two reactions are kinetically indistinguishable in experiments. The total hydrolysis rate v is given by

$$v = k_1[\text{cAMP}^-][\text{HO}^-] + k_2[\text{cAMP}^-][\text{H}_2\text{O}] + k_3[\text{cAMPH}][\text{HO}^-] + k_4[\text{cAMPH}][\text{H}_2\text{O}] \quad (5)$$

in which k_1, k_2, k_3, and k_4 are the rate constants and are dependent on the Gibbs free-energy barriers for the corresponding rate-controlling steps. For a given pH, concentrations [H_2O] and [HO^-] are all constants (∼55.5 and 10^{-7} M at pH 7). The relative concentrations of $cAMP^-$ and cAMPH are determined by the pK_a of cAMPH and the pH of the solution. Although we have not found an experimental pK_a value for cAMPH, we expect that the pK_a of cAMPH should not be dramatically different from those of other phosphodiesters. The experimental pK_a of DMPH is known to be 0.99,[35] so which route is dominant is dependent on the relative free-energy barriers, the pK_a of cAMPH, and the pH of the solution. Given the pK_a and pH values, we need only predict the free-energy barriers for all of the possible reaction pathways to know which pathway is dominant.

Our work reported here is aimed at the study of the fundamental reaction pathways and predicts the corresponding free energies for the hydrolysis of cAMP in the gas phase and in aqueous solution. For this purpose, we performed a series of first-principles electronic structure calculations on the hydrolysis of an appropriate cAMP model (Scheme 2). For a key reaction pathway, another phosphodiester (i.e., trimethylene phosphate (TMP), which is the parent six-membered phosphodiester and can be considered to be a more simplified model of cAMP) was also examined to verify that the used cAMP model is sufficiently large and that the used computational methods are reliable for the prediction of the fundamental pathways and activation data. The calculated results provide useful insights into the fundamental reaction mechanism and kinetics for the hydrolysis of cAMP and related phosphodiesters.

SCHEME 2: Hydrolysis of the cAMP Model and Its Protonated Form

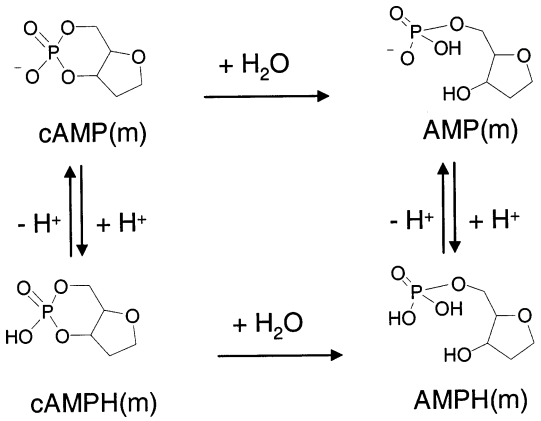

Calculation Methods

For all reactions under consideration in this study, we first employed the Hartree−Fock (HF) method and the 3-21+G(*) basis set[36] to search for and optimize all possible geometries of transition states and intermediates as well as reactants and products. The geometries obtained at the HF/3-21+G(*) level were then refined at the HF/6-31+G(d) level.[36] Vibrational frequency calculations were carried out to ensure that the geometries are indeed local minima or saddle points on the potential energy surfaces and to determine the zero-point vibration energies and thermal corrections to the Gibbs free energies. Intrinsic reaction coordinate (IRC)[37] calculations were performed at the HF/6-31+G(d) level to confirm the correct connections between the stationary points associated with the transition states, intermediates, reactants, and products on the potential energy surfaces. The geometries optimized at the HF/6-31+G(d) level were employed to perform the second-order Møller−Plesset (MP2) energy calculations with the 6-31+G(d) basis set.

Previous theoretical studies[17,38,39] of reaction pathways for hydroxide ion-catalyzed ester hydrolyses indicate that electron correlation effects are not important in the optimizations of molecular geometries and calculations of solvent shifts but are important in final energy calculations for studying the energy profiles of those organic reactions. With a given basis set, the energy barriers evaluated by performing the MP2 energy calculations using the MP2 geometries are all very close to those evaluated by the MP2 calculations using geometries optimized with the HF and density functional theory (DFT) methods. The energy barriers calculated with the MP2 method are all very close to those calculated with the MP4SDQ, QCISD, and QCISD(T) methods,[38] indicating that the MP2 method is sufficiently accurate for the recovery of electron correlation. Regarding the basis set dependence, the energy barriers determined with the 6-31+G(d) basis set are all very close to

those determined with the 6-31++G(d,p) and 6-311++G(3d,3p) basis sets.[17,38] To examine further the accuracy of the energy barriers calculated at the MP2/6-31+G(d)//HF/6-31+G(d) level, in the present study, additional single-point energy calculations were performed at the MP2/6-31++G(d,p)//HF/6-31+G(d) level on all geometries for the determined most important reaction pathway.

Solvent effects were accounted for by performing self-consistent reaction field (SCRF) energy calculations on the geometries optimized at the HF/6-31+G(d) level in the gas phase. The calculated free-energy change in aqueous solution was taken as the energy change calculated at the MP2/6-31+G(d) level in the gas phase with the HF/6-31+G(d) zero-point and other thermal corrections (at 298 K and 1 atm) plus the corresponding solvent shift calculated by performing SCRF calculations at the HF/6-31+G(d) level. A recently developed SCRF method, known as the surface and volume polarizations for electrostatics (SVPE),[40−43] implemented in a local version[40] of the GAMESS program,[44] was used in the solvation calculations. This SVPE method is also known as the fully polarizable continuum model (FPCM)[15a,39,45] because it fully accounts for both surface and volume polarization effects in the solute−solvent electrostatic interaction. Some advantages of the SVPE method over other SCRF methods can be found in our previous reaction field calculations by using various SCRF methods on the energy barriers of a series of carboxylic acid esters.[43]

According to the SVPE procedure,[40] the solute cavity surface is defined as a solute charge isodensity contour determined self-consistently during the SVPE iteration process, and the numerical results of the SVPE calculation can converge to the exact solution of Poisson's equation with a given numerical tolerance. The converged SVPE results are dependent only on the contour value at a given dielectric constant and a certain quantum mechanical calculation level.[40] By seeking the best overall agreement with experimental conformational free-energy differences (62 experimental observations) in various polar solutes existing in various solvents, this single-parameter value has been calibrated as 0.001 au.[41] By seeking the best overall agreement with experimental ^{15}N NMR chemical shifts (48 experimental observations) in various polar solutes existing in various solvents, this single-parameter value has been calibrated as 0.002 au.[42] Nevertheless, for both the experimental conformational free-energy differences and the NMR chemical shifts, the SVPE results with the 0.002 au contour are very close to the corresponding SVPE results with the 0.001 au contour. On the basis of the fitting process employed in the calibration, the root-mean-square (rms) deviations of the 62 experimental values for the conformational free-energy differences from the results calculated by the SVPE method using the 0.001 and 0.002 au contours are 0.096 and 0.104 kcal/mol^{-1}, respectively.[41] The root-mean-square (rms) deviations of the 48 experimental values for the NMR chemical shifts from the results calculated by the SVPE method using the 0.001 and 0.002 au contours are 2.6 and 2.3 ppm, respectively.[42] Obviously, the 0.001 and 0.002 au contours are all acceptable for the SVPE calculations on both kinds of properties. Compared to the solvation calculations neglecting volume polarization, the SVPE results are rather insensitive to the cavity size that is used.[42] Recent SVPE calculations on the hydroxide ion-catalyzed hydrolysis of a series of carboxylic acid esters indicated that the energy barriers determined by the SVPE calculations using both the 0.001 and 0.002 au contours are all qualitatively consistent with the corresponding experimental activation energies.[39,43] The SVPE calculations using the 0.001 au contour slightly and systematically underestimate the energy barriers, whereas the differences between values from the SVPE calculations using the 0.002 au contour and the corresponding average experimental values for the examined esters are smaller than the range of experimental values reported by different laboratories.[43] So both the 0.002 au contour and the default 0.001 au contour were used in this study for further comparison to examine whether such a change to the default 0.001 au contour can significantly change the calculated energy barriers or not. The dielectric constant of water used for the solvation calculations is 78.5.

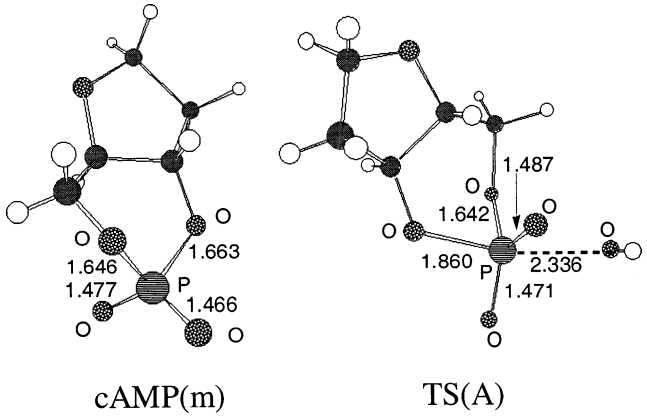

Figure 1. Geometries of the reactant cAMP(m) and the transition state optimized at the HF/6-31+G(d) level for the pathway associated with reaction 1.

All of the gas-phase calculations were performed by using the Gaussian 98 program,[46] and all of the solvation calculations were carried out by using a local version of the GAMESS program.[44]

Results and Discussion

Reaction Coordinates and Geometries. We examined a total of four possible types of hydrolysis pathways associated with reactions 1 to 4. The first type, associated with reaction 1, is the hydroxide ion-catalyzed hydrolysis of the anionic structural form. Our reaction coordinate calculations indicate that reaction 1 occurs by the attack of the hydroxide oxygen at the phosphorus center to form a transition state. Whereas the oxygen atom of the hydroxide ion gradually approaches the phosphorus atom, the ester oxygen gradually leaves the phosphorus atom in the opposite direction. The optimized geometries of the reactant (i.e., the cAMP model denoted by cAMP(m)) and the transition state denoted by TS(A) are depicted in Figure 1 along with some key geometrical parameters. The IRC calculation in one direction went to reactants cAMP(m) + HO^-. The IRC calculation in another direction went directly to the product without going through a pentacoordinated phosphorus intermediate. It should be mentioned that our geometry optimizations and IRC calculations were all performed in the gas phase. Florian and Warshel[23] performed a manual geometry search in solution along the corresponding gas-phase intrinsic reaction coordinate for the hydrolysis of monomethyl phosphate and demonstrated that the contributions of the solvent-induced conformational changes to the overall energetics are small and can be safely neglected.

Our IRC results are qualitatively consistent with the results reported for smaller phosphate diesters by Lim et al.[25,26] and more recently by Florian et al..[24] Whereas Lim et al. carried out the geometry optimizations in the gas phase for both cyclic and acyclic diesters,[25,26] Florian et al. performed geometry optimization in solution at the HF/6-31G(d) level for DMP.[24] The ab initio calculations reported by Lim, Dejaegere, and

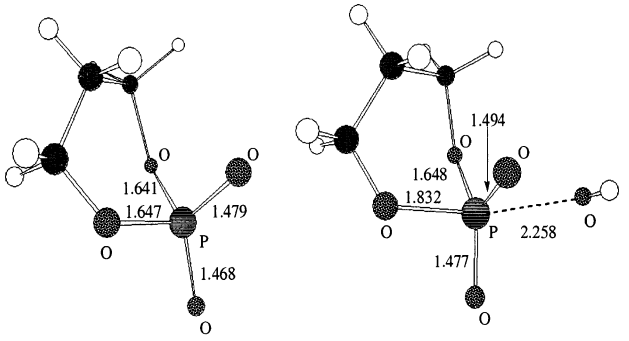

Figure 2. Geometries of the reactant TMP and the transition state optimized at the HF/6-31+G(d) level for the pathway associated with reaction 2.

Karplus[25,26] were performed at the HF/STO-3G, HF/3-21G(*), and HF/3-21+G(*) levels. According to their results calculated at the HF/STO-3G level, the dianionic pentacoordinated phosphorus intermediate exists during the hydrolysis for both the cyclic and acyclic esters. According to their results calculated at the HF/3-21G(*) and HF/3-21+G(*) levels, the dianionic pentacoordinated phosphorus intermediate exists for the acyclic ester (with a negligible energy barrier) but does not exist for the cyclic ester. Our ab initio calculations at the higher level (with the larger basis set) are consistent with the conclusion[24−26] of the nonexistence of the dianionic pentacoordinated phosphorus intermediate during the base-catalyzed hydrolysis of cyclic phosphate ester. So reaction 1 is a one-step process, S_N2, involving only one transition state. Such a one-step reaction pathway also exists for the hydroxide ion-catalyzed hydrolysis of TMP. TMP may be regarded as a more simplified model of cAMP. The optimized geometries of TMP and the transition state, TS(TMP), are depicted in Figure 2. The difference between TMP and cAMP(m) is that the five-membered ring in cAMP(m) does not exist in TMP.

Possible pathways associated with reactions 2 and 3 were examined carefully by using various different initial geometries in the geometry optimizations of the first transition states. We expected to find two different transition states for the first reaction step; one is associated with reaction 2, and the other is associated with reaction 3. However, the geometry optimizations starting from different initial geometries all eventually went to the same transition-state structure, TS1(B) depicted in Figure 3. The optimized TS1(B) geometry looks like a transition state associated with reaction 3. Surprisingly, the IRC calculation starting from transition state TS1(B) went to the reactants cAMP(m) + H_2O, rather than cAMPH(m) + HO^-, in the backward direction. So transition state TS1(B) is actually associated with reaction 2 rather than reaction 3. The calculated results suggest that for reaction 3 to occur cAMPH(m) will first need to transfer a proton to HO^-,

$$\text{cAMPH(m)} + HO^- \rightarrow \text{cAMP(m)} + H_2O \qquad (6)$$

so that reactants cAMPH(m) + HO^- become cAMP(m) + H_2O before the hydrolysis.[47] The hydrolysis starting from cAMP(m) + H_2O is actually associated with reaction 2, so reaction 2 can actually be regarded as part of reaction 3. The IRC calculation in the forward direction went to a pentacoordinated phosphorus intermediate, denoted by INT1(B) depicted in Figure 3. The pentacoordinated phosphorus has a distorted trigonal bipyramidal coordination structure with two axial oxygen atoms and three equatorial oxygen atoms. In INT1(B), the attacking oxygen atom and the ester oxygen that will leave the P atom later stay in the axial direction. The remaining three oxygen atoms coordinating to the P atom all stay in the equatorial direction, so the first step of reaction 2 is initialized by the attack of the water oxygen at the phosphorus center. Whereas the water oxygen gradually approaches the phosphorus atom, a hydrogen atom in the water molecule gradually transfers to a negatively charged equatorial oxygen atom of cAMP(m). In intermediate INT1(B), the proton has already been transferred.

The decomposition of the pentacoordinated phosphorus intermediate to product AMP(m) is associated with the breaking of the axial P−O bond involving an ester oxygen. Breaking the axial P−O bond requires a proton transfer from a hydroxyl group to the leaving ester oxygen, so the second step of reaction 2 is the rotation of the equatorial P−OH bond. Through the rotation, a hydrogen bond between the two hydroxyl groups in INT1(B) gradually breaks, and another hydrogen bond between the equatorial hydroxyl group and the axial ester oxygen gradually forms in a new pentacoordinated phosphorus intermediate denoted by INT2(B). Between the two intermediate structures, there exists a rotational transition state, denoted by TSrot(B) depicted in Figure 3. The third step of reaction 2, starting from INT2(B), is the concurrent axial ester oxygen leaving and proton transfer from the equatorial hydroxyl to the leaving oxygen. The transition state corresponding to this reaction step is TS2(B), which is depicted in Figure 3.

Reaction 4 was found to be associated with a two-step process. The first step is the formation of a pentacoordinated phosphorus intermediate. This step is associated with a water oxygen attacking at P atom of cAMPH(m) while a proton transfers from the water oxygen to the phosphoryl oxygen. The second step of the reaction is the decomposition of the intermediate to AMPH(m). In this step, the axial ester oxygen gradually leaves the P atom while a proton gradually transfers from the equatorial hydroxyl to the leaving oxygen. The optimized geometries of the two transition states (i.e., TS1(C) and TS2(C)) and the pentacoordinated phosphorus intermediate (i.e., INT(C)) are depicted in Figure 4.

In light of the theoretical results obtained from the reaction coordinate calculations, eq 5 may be rewritten as

$$v = k_1[\text{cAMP}^-][HO^-] + k_2[\text{cAMP}^-][H_2O] + k_4[\text{cAMPH}][H_2O] \qquad (7)$$

Energetics and Kinetics. On the basis of the optimized geometries of the transition states, intermediates, and reactants, we calculated the energy barriers (activation energies) and Gibbs free-energy barriers (activation free energies) in the gas phase and in aqueous solution. The activation data calculated for cAMP(m) hydrolysis are summarized in Table 1. As seen in Table 1, the energy barriers and free-energy barriers calculated for reaction 1 at the MP2/6-31++G(d,p) level are lower than the corresponding values calculated at the MP2/6-31+G(d) level by only ~0.2 kcal/mol. This suggests that the 6-31+G(d) basis set used in our calculations is indeed sufficient for these reaction systems.

Concerning the reliability of the solvation calculations, the data in Table 1 show that the energy barriers and free-energy barriers calculated with the SVPE method using the 0.002 au contour are close to the corresponding values with the SVPE method using the default 0.001 au contour, particularly for reaction 1. Reaction 1 is the hydroxide ion-catalyzed hydrolysis, the primary pathway concerned in this study. The differences

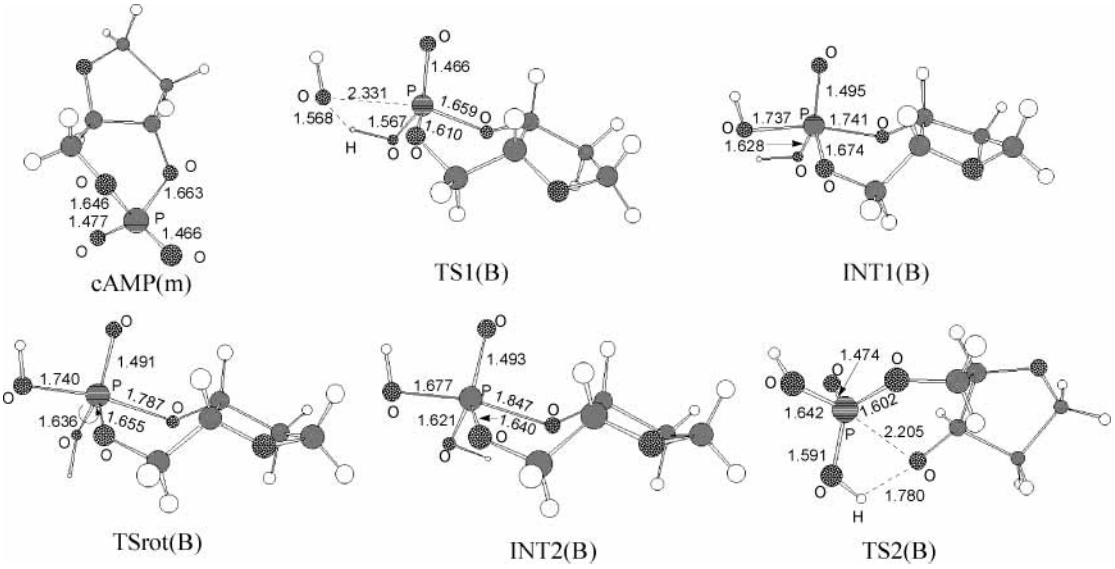

Figure 3. Geometries of the reactant cAMP(m), transition states, and intermediates optimized at the HF/6-31+G(d) level for the pathway associated with reaction 2.

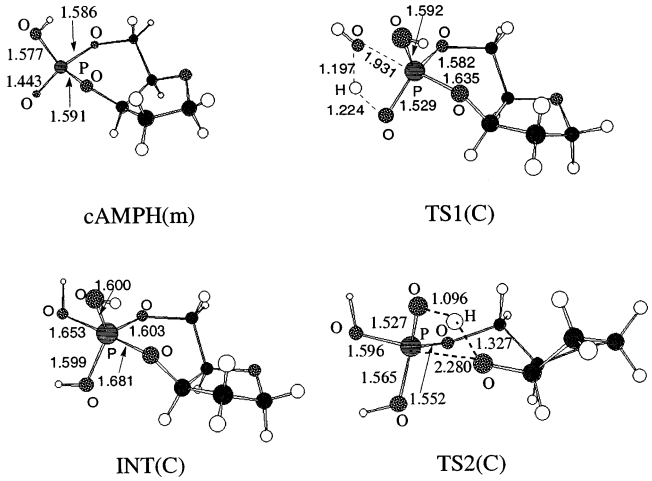

Figure 4. Geometries of the reactant cAMPH(m), transition states, and intermediates optimized at the HF/6-31+G(d) level for the pathway associated with reaction 4.

between these two sets of SVPE results are within ~0.6 kcal/mol for the hydroxide ion-catalyzed hydrolysis of cAMP(m). As seen in Table 1, the Gibbs free-energy barrier for the hydroxide ion-catalyzed hydrolysis of cAMP(m) was calculated to be 29.6 kcal/mol with the default 0.001 au contour and 30.2 kcal/mol with the 0.002 au contour. The difference is ~0.6 kcal/mol. In comparison, the Gibbs free-energy barrier for the hydroxide ion-catalyzed hydrolysis of TMP was calculated to be 32.0 kcal/mol with the default 0.001 au contour and 32.2 kcal/mol with the 0.002 au contour. The difference is only ~0.2 kcal/mol. For the other reaction pathways, the differences become slightly larger (~1.7 to 2.0 kcal/mol), as seen from the data in Table 1; these differences do not significantly change the relative energetic results. This suggests that the SVPE calculations using the default 0.001 au contour are adequate for this study. The discussion below refers only to the results calculated with the default 0.001 au contour. Unless clearly specified otherwise, all activation data discussed below refer to cAMP(m).

Compared to the free-energy barrier calculated for the hydroxide ion-catalyzed hydrolysis of TMP in aqueous solution, the free-energy barrier calculated for the hydroxide ion-catalyzed hydrolysis of cAMP(m) in aqueous solution is ~2 kcal/mol lower. The shift of ~ −2 kcal/mol is attributed to the effects of an extra five-membered ring in cAMP(m). This shift is certainly significant but not dramatic. The absolute value of the free-energy barrier shift from cAMP(m) to cAMP is expected to be smaller than the ~2 kcal/mol shift from TMP to cAMP(m) because the structural difference between cAMP(m) and cAMP is farther from the reaction center. Therefore, cAMP(m) can be considered to be an adequate model of cAMP, and the results calculated for cAMP(m) should give some useful insights into the hydrolysis of cAMP. Below we discuss the cAMP hydrolysis by using the energetic results calculated for cAMP(m).

For the gas-phase reactions, reaction 1 has a very high energy barrier (~80.0 kcal/mol) and free-energy barrier (~89.0 kcal/mol) according to our calculations. For the three steps of reaction 2, the highest energy barrier (~26.3 kcal/mol) and free-energy barrier (~36.4 kcal/mol) are always associated with the first step. For the two steps of reaction 4, the highest free-energy barrier (~32.2 kcal/mol) is associated with the first step, although the highest energy barrier (~21.2 kcal/mol) is associated with the second step in the gas phase. So the first step is always rate-controlling for each reaction pathway, and comparisons of the hydrolysis rate between different reaction pathways should focus on the free-energy barriers for the first steps. The calculated free-energy barriers in Table 1 predict that for the three reactions in the gas phase reaction 4 is the fastest because the free-energy barrier (~32.2 kcal/mol) for its rate-controlling step is the lowest and reaction 1 is the slowest because its free-energy barrier (~89.0 kcal/mol) is the highest.

The solvent effects dramatically change the relative free-energy barriers for the rate-controlling steps and therefore the relative reaction rates. The calculated largest absolute value of the solvent shift of the free-energy barrier is as high as 49.4 kcal/mol. As a result, for the hydrolysis in aqueous solution reaction 1 is associated with the lowest energy barrier and the free-energy barrier, as compared to those for the rate-controlling steps of the other two reactions in solution. The free-energy barrier of 29.6 kcal/mol calculated for reaction 1 is lower than that for reaction 2 by 16.4 kcal/mol and that for reaction 4 by 15.8 kcal/mol. These values indicate that $k_1/k_2/k_4 \approx 10^{12}$:1:3 according to conventional transition-state theory (CTST):[48]

TABLE 1: Calculated Energy Barriers (ΔE) and Free-Energy Barriers (ΔG) in kcal/mol[a]

	gas phase		solution[c]		solution (0.002)[d]	
reaction	ΔE	ΔG	ΔE	ΔG	ΔE	ΔG
reaction 1						
cAMP(m) + OH^- → TS(A)	80.0 (79.8)[b]	89.0 (88.8)[b]	20.6 (20.4)[b]	29.6 (29.4)[b]	21.2 (21.0)[b]	30.2 (30.0)[b]
reaction 2						
cAMP(m) + H_2O → TS1(B)	26.3	36.4	35.9	46.0	37.9	48.0
INT1(B) → TSrot(B)	10.1	9.7	7.7	7.2	6.5	6.0
INT2(B) → TS2(B)	2.9	2.8	6.0	5.9	6.4	6.3
reaction 3						
cAMPH(m) + H_2O → TS1(C)	21.2	32.2	34.4	45.4	36.1	47.1
INT(C) → TS2(C)	24.7	23.8	20.6	19.7	20.7	19.8

[a] All energy calculations were performed by using the geometries optimized at the HF/6-31+G(d) level. Unless otherwise indicated, the gas-phase energy calculations are determined at the MP2/6-31+G(d) level. The energy barriers include the zero-point energy corrections. [b] For the values in parentheses, the gas-phase energy calculations were performed at the MP2/6-31++G(d,p) level. [c] The solution results are based on the solvent shifts determined by the SVPE calculations with the default 0.001 au contour. [d] The solution results are based on the solvent shifts determined by the SVPE calculations with the 0.002 au contour.

$$k = \left(\frac{k_B T}{h}\right) \exp\left(\frac{-\Delta G}{k_B T}\right) \quad (8)$$

where k_B is the Boltzmann constant, T is the absolute temperature, h is Planck's constant, and ΔG is the free-energy barrier.

We note that the relative contributions of different reaction pathways to the total hydrolysis rate, υ in eq 7, are determined not only by the relative free-energy barriers but also by the relative concentrations of the involved reactants. The ratio of $[HO^-]$ to $[H_2O]$ is determined by the pH of the reaction solution. At pH 7, $[HO^-]/[H_2O] \approx 10^{-7}/55.5 \approx 2 \times 10^{-8}$. The ratio of [cAMPH] to $[cAMP^-]$ is determined by both the pK_a of cAMPH and the pH of the solution. For example, assuming that the pK_a of cAMPH is close to the experimental pK_a value of DMPH, ~1, we should have $[cAMPH]/[cAMP^-] = \sim 10^{-6}$ at pH 7. Under this condition, we obtain

$$k_1[cAMP^-][HO^-]/k_2[cAMP^-][H_2O]/k_4[cAMPH][H_2O] \approx 2 \times 10^4{:}1{:}3 \times 10^{-6} \quad (9)$$

So at pH 7, the contribution of reaction 4 to the total hydrolysis rate should be the smallest so long as the pK_a of cAMPH is not larger than ~6.5; we are not aware of any phosphodiester with a pK_a value as large as ~6.5. In the unlikely case of pK_a(cAMPH) = ~6.5, we would have $k_2[cAMP^-][H_2O] \approx k_4[cAMPH][H_2O]$. It follows that reactions 1 and 2 represent the two main reaction pathways for the hydrolysis of cAMP in aqueous solution when the pH of the solution is around 7.

Depicted in Figure 5 is the pH dependence of the $\log\{k_1[cAMP^-][HO^-]\}$, $\log\{k_2[cAMP^-][H_2O]\}$, and $\log\{k_4[cAMPH][H_2O]\}$ values calculated by using CTST and some additional assumptions. According to CTST, we can evaluate the rate constants only for a given temperature T and the free-energy barriers calculated for the solution reactions at the MP2/6-31+G(d)//HF/6-31+G(d) level. We used $T = 298.15$ K. In addition, we further assumed that $[cAMP^-] + [cAMPH] = 1$ M and pK_a = 1 for cAMPH in our calculations. As seen in Figure 5, when the pH of the solution increases, $k_1[cAMP^-][HO^-]$ increases whereas $k_4[cAMPH][H_2O]$ decreases. The $k_2[cAMP^-][H_2O]$ value increases with increasing pH when the pH is very low and is constant when the pH is significantly higher than ~2. The $k_4[cAMPH][H_2O]$ value is larger than those of $k_1[cAMP^-][HO^-]$ and $k_2[cAMP^-][H_2O]$ only for pH < ~1.3, so the contribution of reaction 4 is the largest only for pH < ~1.3.

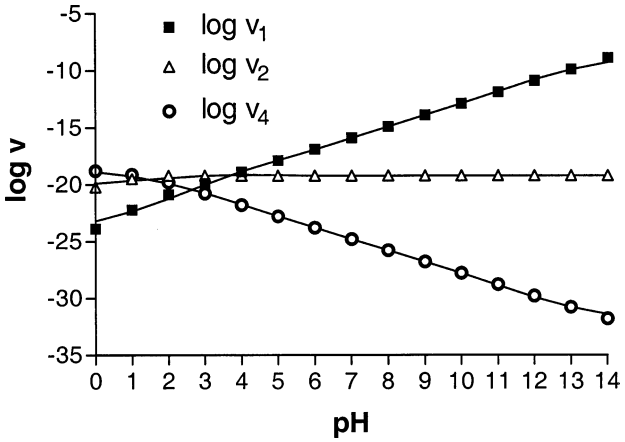

Figure 5. Calculated values of log υ_1, log υ_2, and log υ_4 versus the pH of the reaction solution at $T = 298.15$ K. $\upsilon_1 = k_1[cAMP^-][HO^-]$, $\upsilon_2 = k_2[cAMP^-][H_2O]$, and $\upsilon_4 = k_4[cAMPH][H_2O]$.

For ~1.3 < pH < ~3.7, $k_2[cAMP^-][H_2O]$ has the largest value; therefore, the contribution of reaction 2 is the largest. At pH ~3.7, we have $k_1[cAMP^-][HO^-] \approx k_2[cAMP^-][H_2O]$. At pH > ~3.7, the contribution of reaction 1 is the largest. We are particularly interested in the hydrolysis of cAMP under physiological conditions at pH ~7 (neutral aqueous solution). Reaction 1 should be the dominant pathway for cAMP hydrolysis in a neutral aqueous solution. This theoretical conclusion is consistent with a recent experimental study[49] providing isotopic evidence for direct attack by hydroxide ion in the alkaline hydrolysis of another phosphodiester **(**with a *p*-nitrophenolate leaving group).

Finally, now that the hydroxide ion-catalyzed hydrolysis has been determined to be the dominant pathway in neutral aqueous solution, the reliability of our theoretical predictions can further be examined by comparison between the available experimental data and the results calculated for the hydroxide ion-catalyzed reaction pathway for TMP hydrolysis. Reported experimental kinetic data have shown that EP hydrolyzes about 10^7 as fast as does DMP,[50] whereas TMP hydrolyzes "at very nearly the same rate as an acyclic ester" such as DMP.[51] Because the experimental estimate of the activation free energy used in the literature for the alkaline hydrolysis of DMP is 32 kcal/mol,[32] the experimental estimate of the activation free energy for the alkaline hydrolysis of TMP should be close to ~32 kcal/mol according to conventional transition-state theory.[48] The estimated

activation free energy of ~32 kcal/mol is in excellent agreement with our predicted free-energy barrier of 32.0 kcal/mol for the dominant hydroxide ion-catalyzed hydrolysis of TMP. This agreement further suggests that we have provided a reliable computational prediction of the fundamental reaction pathways and corresponding activation data for the nonenzymatic hydrolysis of cAMP and related phosphodiesters.

Conclusions

A series of first-principles electronic structure calculations have been performed to study possible competing reaction pathways and the corresponding free-energy barriers for the ester hydrolysis of intracellular second-messenger adenosine 3′,5′-cyclic monophosphate (cAMP) and related phosphodiesters. The reaction coordinate calculations reveal three fundamental reaction pathways for the ester hydrolysis: (A) attack of a hydroxide ion at the phosphorus center of the anion (i.e., the hydroxide ion-catalyzed hydrolysis); (B) direct attack of a water molecule at the phosphorus center of the phosphate anion; and (C) direct attack of a water molecule at the phosphorus center of the protonated structure (i.e., the neutral ester molecule). Reaction pathway A is actually a single-step S_N2 process without the existence of a pentacoordinated phosphorus intermediate. Pathway B is a three-step process involving two pentacoordinated phosphorus intermediate structures. Pathway C is a two-step process with a single pentacoordinated phosphorus intermediate structure.

The calculated energetic results indicate that the first step of the reaction is always the rate-controlling step for all of the multiple-step pathways. For the reactions in the gas phase, the calculated free-energy barrier for pathway A is the highest, and that for the rate-controlling step of pathway C is the lowest. The solvation effects dramatically change the calculated free-energy barriers such that the free-energy barrier calculated for pathway A becomes the lowest and the two main reaction pathways are A and B for the hydrolysis in aqueous solution.

We also have demonstrated how the pK_a of the ester and the pH of the reaction solution affect the relative contributions of different reaction pathways to the total hydrolysis rate. It has been shown that reaction pathway A should be dominant for cAMP hydrolysis in neutral aqueous solution (pH 7). However, the relative contribution of pathway A to the total hydrolysis rate should decrease with the decreasing pH of the solution. For pH < ~3.7, the contribution of pathway B is larger. For pH > ~3.7, the contribution of pathway A is larger.

In addition, the reliability of our theoretical predictions is supported by the excellent agreement between the calculated free-energy barrier for the hydroxide ion-catalyzed hydrolysis of TMP in aqueous solution and the available experimental kinetic data.

Supporting Information Available: Individual energies calculated by using the geometries optimized at the HF/6-31+G(d) level. This includes the total energy, zero-point vibrational energy, thermal correction to the Gibbs free energy calculated at the HF/6-31+G(d) level in the gas phase, total energy calculated at the MP2/6-31+G(d)//HF/6-31+G(d) level in the gas phase, and energies calculated by using the FPCM method at the HF/6-31+G(d) level in solution for each structure depicted in Figures 1 to 4. This material is available free of charge via the Internet at http://pubs.acs.org.

References and Notes

(1) Sutherland, E. W.; Rall, T. W. *J. Biol. Chem.* **1958**, *232*, 1065.
(2) Callahan, S. M.; Cornell, N. W.; Dunlap, P. V. *J. Biol. Chem*. **1995**, *270*, 17627.
(3) Xu, R. X.; Hassell, A. M.; Vanderwall, D.; Lambert, M. H.; Holmes, W. D.; Luther, M. A.; Rocque, W. J.; Milburn, M. V.; Zhao, Y.; Ke, H.; Nolte, R. T. *Science* **2000**, *288*, 1822.
(4) Sung, B.-J.; Hwang, K. Y.; Jeon, Y. H.; Lee, Jae I.; Heo, Y.-S.; Kim, J. H.; Moon, J.; Yoon, J. M.; Hyun, Y.-L.; Kim, E.; Eum, S. J.; Park, S.-Y.; Lee, J.-O.; Lee, T. G.; Ro, S.; Cho, J. M. *Science* **2003**, *425*, 98.
(5) Conti, M.; Jin, S. L. C.; Monaco, L.; Repaske, D. R.; Swinnen, J. V. *Endocr. Rev.* **1991,** *12*, 218.
(6) Teixeira, M. M.; Gristwood, R. W.; Cooper, N.; Hellewell, P. G. *Trends Pharmacol. Sci.* **1997**, *18*, 164.
(7) Houslay, M. D.; Sullivan, M.; Bolger, G. B. *Adv. Pharmacol*. **1998**, *44*, 225.
(8) Weishaar, R. E.; Cain, M. H.; Bristol, J. A. *J. Med. Chem*. **1985**, *28*, 537.
(9) (a) Burnouf, C.; Auclair, E.; Avenel, N.; Bertin, B.; Bigot, C.; Calvet, A.; Chan, K.; Durand, C.; Fasquelle, V.; Feru, F.; Gilbertsen, R.; Jacobelli, H.; Kebsi, A.; Lallier, E.; Maignel, J.; Martin, B.; Milano, S.; Ouagued, M.; Pascal, Y.; Pruniaux, M.-P.; Puaud, J.; Rocher, M.-N.; Terrasse, C.; Wrigglesworth, R.; Doherty, A. M. *J. Med. Chem.* **2000**, *43*, 4850. (b) Ukita, T.; Nakamura, Y.; Kubo, A.; Yamamoto, Y.; Moritani, Y.; Saruta, K.; Higashijima, T.; Kotera, J.; Takagi, M.; Kikkawa, K.; Omori, K. *J. Med. Chem.* **2001**, *44*, 2204. (c) Van der Mey, M.; Boss, H.; Couwenberg, D.; Hatzelmann, A.; Sterk, G. J.; Goubitz, K.; Schenk, H.; Timmerman, H. *J. Med. Chem.* **2002**, *45*, 2526. (d) Friesen, R. W.; Ducharme, Y.; Ball, R. G.; Blouin, M.; Boulet, L.; Cote, B.; Frenette, R.; Girard, M.; Guay, D.; Huang, Z.; Jones, T. R.; Laliberte, F.; Lynch, J. J.; Mancini, J.; Martins, E.; Masson, P.; Muise, E.; Pon, D. J.; Siegl, P. K. S.; Styhler, A.; Tsou, N. N.; Turner, M. J.; Young, R. N.; Girard, Y. *J. Med. Chem.* **2003**, *46*, 2413.
(10) Houslay, M. D. *Semin. Cell Dev. Biol*. **1998**, *9*, 161.
(11) Londesborough, J. *Biochem. J*. **1985**, *225*, 143.
(12) Marchmont, R. J.; Houslay, M. D. *Nature* **1980**, *286*, 904.
(13) Marchmont, R. J.; Ayad, S. R.; Houslay, M. D. *Biochem. J*. **1981**, *195*, 645.
(14) Francis, S. H.; Colbran, J. L.; McAllister-Lucas, L. M.; Corbin, J. D. *J. Biol. Chem*. **1994**, *269*, 22477.
(15) (a) Zhan, C.-G.; Norberto de Souza, O.; Rittenhouse, R.; Ornstein, R. L. *J. Am. Chem. Soc.* **1999**, *121*, 7279. (b) Koca, J.; Zhan, C.-G.; Rittenhouse, R.; Ornstein, R. L. *J. Am. Chem. Soc*. **2001**, *123*, 817. (c) Koca**,** J.; Zhan, C.-G.; Rittenhouse, R. C.; Ornstein, R. L. *J. Comput. Chem.* **2003**, *24*, 368.
(16) Zhan, C.-G.; Zheng, F. *J. Am. Chem. Soc.* **2001**, *123*, 2835.
(17) Zheng, F.; Zhan, C.-G.; Ornstein, R. L. *J. Chem. Soc., Perkin Trans. 2* **2001**, 2355.
(18) (a) Westheimer, F. H. *Chem. Rev.* **1981**, *4*, 313. (b) Hengge, A. C.; Cleland, W. W. *J. Am. Chem. Soc.* **1990**, *112*, 7421.
(19) Admiraal, S. J.; Herschlag, D. *Chem. Biol.* **1995**, *2*, 729.
(20) Maegley, K. A.; Admiraal, S. J.; Herschlag, D. *Proc. Natl. Acad. Sci. U.S.A.* **1996**, *93*, 8160.
(21) Florian, J.; Warshel, A. *J. Am. Chem. Soc.* **1997**, *119*, 5473.
(22) Aqvist, J.; Kolmodin, K.; Florian, J.; Warshel, A. *Chem. Biol.*, **1999**, *6*, R71.
(23) Florian, J.; Warshel, A. *J. Phys. Chem. B* **1998**, *102*, 719.
(24) Florian, J.; Goodman, M. F.; Warshel, A. *J. Am. Chem. Soc.* **2003**, *125*, 8163.
(25) Lim, C.; Karplus, M. *J. Am. Chem. Soc.* **1990**, *112*, 5872.
(26) Dejaegere, A.; Lim, C.; Karplus, M. *J. Am. Chem. Soc.* **1991**, *113*, 4353.
(27) Lim, C.; Tole, P. *J. Phys. Chem.* **1992**, *96*, 5217.
(28) Tole, P.; Lim, C. *J. Phys. Chem.* **1993**, *97*, 6212.
(29) Tole, P.; Lim, C. *J. Am. Chem. Soc.* **1994**, *116*, 3922.
(30) Chang, N.-Y.; Lim, C. *J. Am. Chem. Soc.* **1998**, *120*, 2167.
(31) Yliniemela, A.; Uchimaru, T.; Tanabe, K.; Taira, K. *J. Am. Chem. Soc*. **1993**, *115*, 3032.
(32) Dejaegere, A.; Karplus, M. *J. Am. Chem. Soc.* **1993**, *115*, 5316.
(33) Dejaegere, A.; Liang, X. L.; Karplus. M. *J. Chem. Soc., Faraday Trans.* **1994**, *90*, 1763.
(34) Lopez, X.; Dejaegere, A.; Karplus, M. *J. Am. Chem. Soc.* **2001**, *123*, 11755.
(35) Lopez, X.; Schaefer, M.; Dejaegere, A.; Karplus, M. *J. Am. Chem. Soc.* **2002**, *124*, 5010.
(36) Hehre, W. J.; Radom, L.; Schleyer, P. v. R.; Pople, J. A. *Ab Initio Molecular Orbital Theory*; Wiley & Sons: New York, 1986.
(37) (a) Gonzalez, C.; Schlegel, H. B. *J. Chem. Phys*. **1989**, *90*, 2154. (b) Gonzalez, C.; Schlegel, H. B. *J. Phys. Chem*. **1990**, *94*, 5523.
(38) Zhan, C.-G.; Landry, D. W.; Ornstein, R. L. *J. Am. Chem. Soc.* **2000**, *122*, 1522.
(39) (a) Zhan, C.-G.; Landry, D. W.; Ornstein, R. L. *J. Am. Chem. Soc.* **2000**, *122*, 2621. (b) Zhan, C.-G.; Landry, D. W. *J. Phys. Chem. A* **2001**, *105*, 1296.

(40) Zhan, C.-G.; Bentley, J.; Chipman, D. M. *J. Chem. Phys*. **1998**, *108*, 177.
(41) Zhan, C.-G.; Chipman, D. M. *J. Chem. Phys*. **1998**, *109*, 10543.
(42) Zhan, C.-G.; Chipman, D. M. *J. Chem. Phys*. **1999**, *110*, 1611.
(43) Zhan, C.-G.; Landry, D. W.; Ornstein, R. L. *J. Phys. Chem. A* **2000**, *104*, 7672.
(44) Schmidt, M. W.; Baldridge, K. K.; Boatz, J. A.; Elbert, S. T.; Gordon, M. S.; Jensen, J. H.; Koseki, S.; Matsunaga, N.; Nguyen, K. A.; Su, S. J.; Windus, T. L.; Dupuis, M.; Montgomery, J. A. *J. Comput. Chem.* **1993**, *14*, 1347.
(45) (a) Zhan, C.-G.; Niu, S.; Ornstein, R. L. *J. Chem. Soc., Perkin Trans. 2* **2001**, *1*, 23. (b) Zhan, C.-G.; Dixon, D. A. *J. Phys. Chem. A* **2001**, *105*, 11534. (c) Dixon, D. A.; Feller, D.; Zhan, C.-G.; Francisco, J. S. *J. Phys. Chem. A* **2002**, *106*, 3191. (d) Zheng, F.; Zhan, C.-G.; Ornstein, R. L. *J. Phys. Chem. B* **2002**, *106*, 717. (e) Zhan, C.-G.; Dixon, D. A. *J. Phys. Chem. A* **2002**, *106*, 9737. (f) Zhan, C.-G.; Dixon, D. A.; Sabri, M. I.; Kim, M.-S.; Spencer, P. S. *J. Am. Chem. Soc*. **2002**, *124*, 2744. (g) Zhan, C.-G.; Dixon, D. A. *J. Phys. Chem. A* **2003**, *107*, 4403. (h) Zhan, C.-G.; Dixon, D. A.; Spencer, P. S. *J. Phys. Chem. B* **2003**, *107*, 2853. (i) Dixon, D. A.; Feller, D.; Zhan, C.-G.; Francisco, S. F. *Int. J. Mass Spectrom*. **2003**, *227*, 421.
(46) Frisch, M. J.; Trucks, G. W.; Schlegel, H. B.; Scuseria, G. E.; Robb, M. A.; Cheeseman, J. R.; Zakrzewski, V. G.; Montgomery, J. A., Jr.; Stratmann, R. E.; Burant, J. C.; Dapprich, S.; Millam, J. M.; Daniels, A. D.; Kudin, K. N.; Strain, M. C.; Farkas, O.; Tomasi, J.; Barone, V.; Cossi, M.; Cammi, R.; Mennucci, B.; Pomelli, C.; Adamo, C.; Clifford, S.; Ochterski, J.; Petersson, G. A.; Ayala, P. Y.; Cui, Q.; Morokuma, K.; Malick, D. K.; Rabuck, A. D.; Raghavachari, K.; Foresman, J. B.; Cioslowski, J.; Ortiz, J. V.; Stefanov, B. B.; Liu, G.; Liashenko, A.; Piskorz, P.; Komaromi, I.; Gomperts, R.; Martin, R. L.; Fox, D. J.; Keith, T.; Al-Laham, M. A.; Peng, C. Y.; Nanayakkara, A.; Gonzalez, C.; Challacombe, M.; Gill, P. M. W.; Johnson, B. G.; Chen, W.; Wong, M. W.; Andres, J. L.; Head-Gordon, M.; Replogle, E. S.; Pople, J. A. *Gaussian 98*, revision A.7; Gaussian, Inc.: Pittsburgh, PA, 1998.
(47) We note that we are discussing the geometries optimized in the gas phase. Concerning the relative thermodynamic stability of the systems in aqueous solution, the total free energy of cAMP(m) + H_2O should be significantly lower than that of cAMPH(m) + HO^- because the pK_a value of a phosphodiester should be much smaller than the pK_a value of water.
(48) Alvarez-Idaboy, J. R.; Galano, A.; Bravo-Pérez, G.; Ruíz, M. E. *J. Am. Chem. Soc.* **2001**, *123*, 8387.
(49) Cassano, A. G.; Anderson, V. E.; Harris, M. E. *J. Am. Chem. Soc*. **2002**, *124*, 10964.
(50) (a) Kumamoto, J.; Cox, J. R.; Westheimer. F. H. *J. Am. Chem. Soc.* **1956**, *78*, 4858. (b) Haake, P. C.; Westheimer, F. H. *J. Am. Chem. Soc*. **1961**, *83*, 1102.
(51) Khorana, H. G.; Tener, G. M.; Wright, R. S.; Moffatt, J. G. *J. Am. Chem. Soc.* **1957**, *79*, 430.